Journal of Solid State Chemistry 181 (2008) 3236–3242

Contents lists available at ScienceDirect

Journal of Solid State Chemistry

journal homepage: www.elsevier.com/locate/jssc

X-ray and neutron powder diffraction studies of $Ba(Nd_xY_{2-x})CuO_5$

G. Liu [a], Q. Huang [b], J.A. Kaduk [c], Z. Yang [d], C. Lucas [e], W. Wong-Ng [a,*]

[a] Ceramics Division, National Institute of Standards and Technology (NIST), Gaithersburg, MD 20899, USA
[b] NIST Center for Neutron Research, Naperville, IL 60563, USA
[c] INEOS Technologies, Naperville, IL 60563, USA
[d] Yunnan Normal University, Kunming 650092, PR China
[e] Chemistry & Biochemistry Department, University of Maryland, College Park, MD 20742, USA

ARTICLE INFO

Article history:
Received 19 April 2008
Received in revised form
26 June 2008
Accepted 2 August 2008
Available online 13 August 2008

Keywords:
$Ba(Nd_xY_{2-x})CuO_5$
X-ray diffraction patterns
Crystal structure
Orthorhombic 'green phase'
Tetragonal 'brown phase'
Coated conductors

ABSTRACT

$Ba(R,R')_2CuO_5$ (R,R' = lanthanides and Y) plays an important role as a flux-pinning agent in enhancing the superconducting properties of the $Ba_2(R,R')Cu_3O_{6+x}$ (R,R' = lanthanides and Y) coated conductors. Using X-ray diffraction and neutron diffraction, we found that the $Ba(Nd_xY_{2-x})CuO_5$ solid solution adopts two structure types. In the Nd-rich region ($1.8 \leqslant x \leqslant 2.0$), the materials are of brown color (commonly referred to as the 'brown phase'), and the structure is tetragonal with space group *I4/mbm* (no. 127). In the Y-rich region ($0.0 \leqslant x \leqslant 1.4$), the materials are green (commonly referred to as the 'green phase') and the structure is orthorhombic with space group *Pnma* (no. 62). A two-phase region ($1.4 < x < 1.8$) exists between the orthorhombic and tetragonal phases. The crystal chemistry and crystallography of the orthorhombic 'green phase' series, $Ba(Nd_xY_{2-x})CuO_5$ (isostructural to BaY_2CuO_5), are discussed in this paper.

Published by Elsevier Inc.

1. Introduction

Coated conductor research in lanthanide and mixed-lanthanide-containing superconductors of the general chemical formula of $Ba_2(R,R')Cu_3O_{6+x}$ (R,R' = lanthanides and Y) has become increasingly important due to reported improvement of superconducting properties as compared to that of the $Ba_2YCu_3O_{6+x}$ analog [1,2]. Research and development of coated conductors since the 1990s using $Ba_2YCu_3O_{6+x}$ as a prototype material has led to state-of-the-art rolling-assisted biaxially textured substrate (RABiTS) [3–5] and ion beam-assisted deposition (IBAD) [6–8] technologies for producing long-length flexible substrates with multilayered buffers. Deposition of the superconductor layers has been successfully accomplished using techniques such as e-beam deposition [9,10], chemical vapor deposition [11,12], *ex situ* BaF_2 process [13,14], and trifluoroacetate solution [15,16]. With these efforts, there has been significant progress in achieving long-length-coated conductor tapes.

In order to decrease the production cost of coated conductors, it is critical to continuously improve their superconducting properties. Currently active research efforts in this area include the understanding and the choice of appropriate flux-pinning agents for pinning the flux line movement within the superconductor to avoid energy dissipation. A frequently used, effective flux-pinning agent that is compatible with $Ba_2YCu_3O_{6+x}$ is BaY_2CuO_5 (commonly referred to as the 'green phase' [17–30]). By analogy with the $Ba_2YCu_3O_{6+x}$ system, it is possible to use BaR_2CuO_5 and $Ba(R,R')_2CuO_5$ phases as flux-pinning agents for $Ba_2RCu_3O_{6+x}$ and $Ba_2(R,R')Cu_3O_{6+x}$, respectively. However, BaR_2CuO_5 adopts two structure types: when R is large (R = La and Nd), the compound is brown and the structure is tetragonal [28]. With R = Sm, Eu, Gd, Dy, Ho, Er, Tm, Yb, and Lu, the compound is green and the structure is orthorhombic [22]. It is expected that in the mixed-lanthanide systems, the structure of the corresponding $Ba(R,R')_2CuO_5$ phases will depend on the stoichiometry of R and R'. As structure and morphology of grains are some of the features of a material that need to be considered for effective flux-pinning, detailed crystallographic information of the mixed $Ba(R,R')_2CuO_5$ phases is necessary.

The mixed-lanthanide $Ba_2(Nd,Y)Cu_3O_{6+x}$ superconductor has attracted considerable interest in recent years for coated conductor applications [29]; this paper describes the crystal chemistry and crystallographic investigation of the $Ba(Nd,Y)_2CuO_5$ solid solution. We also prepared X-ray powder reference patterns of selected solid solution members of $Ba(Nd,Y)_2CuO_5$ to be included in the powder diffraction file (PDF, produced by ICDD [31]).

* Corresponding author. Fax: +1 301 975 5334.
E-mail address: Winnie.wong-ng@nist.gov (W. Wong-Ng).

0022-4596/$ - see front matter Published by Elsevier Inc.
doi:10.1016/j.jssc.2008.08.002

2. Experimental

2.1. Synthesis

Polycrystalline samples of $Ba(Nd_xY_{2-x})CuO_5$ ($x = 0.4$, 0.8, 1.0, 1.2, 1.4, 1.6, 1.7, 1.8 and 1.9) were prepared by the conventional high-temperature solid-state synthesis technique from commercial $BaCO_3$ (99.99%), Nd_2O_3 (99.9%), Y_2O_3 (99.999%) and CuO (99.99%). Nd_2O_3 powder was calcined in air at 850 °C for 8 h to remove the absorbed moisture. Powders were weighed in stoichiometric proportions, mixed and calcined at 850 °C for 15 h in air to assure the carbonate decomposition, and then reground and reheated at 930–980 °C for 21 days with intermediate grindings and pelletizations. The annealing process was repeated until no further changes were detected in the powder X-ray diffraction patterns.

2.2. X-ray powder diffraction (XRD experiment)

Phase analyses were carried out using a Phillips X-ray powder diffractometer in $\theta-2\theta$ scan mode with Cu$K\alpha$ radiation and equipped with a series of Soller slits and a scintillation counter. The 2θ scanning range was from 12° to 81°, and the step interval was 0.03°. The whole powder diffraction patterns were subsequently fitted using the 'profile matching of the Rietveld analysis' option of the program *FullProf* [32] with constant scale factor. Pseudo-Voigt profile functions were employed and 13 least-squares parameters (zero-point parameter, lattice parameters, profile parameters *U*, *V*, *W*, Shape, *X*, background function parameters (high-order polynominals)) were varied during the refinement process. The reference diffraction patterns of BaY_2CuO_5 (PDF 38-1434) and $BaNd_2CuO_5$ (PDF 42-0497) were used for performing phase identification.

2.3. Neutron powder diffraction (NPD) experiments

To obtain detailed structural information, in particular, the oxygen content of the samples, three members of the $Ba(Nd_xY_{2-x})CuO_5$ series with $x = 0.4$, 0.8, 1.2 were selected for the NPD study. NPD data were collected using the 32 detector BT-1 diffractometer with a Cu (311) monochromator ($\lambda = 1.5403$ Å) at the NIST Center for Neutron Research. Samples were loaded in a 0.5 in. diameter vanadium can. Measurement was made under ambient conditions. The 2θ angular scanning range was from 10° to 160° with steps of 0.05°. Structure refinement was performed using the program GSAS [33] and the initial structure parameters were taken from the report of BaY_2CuO_5 [21]. The neutron scattering lengths for Ba, Nd, Y, Cu, and O are $(0.525, 0.769, 0.775, 0.772, \text{and } 0.585) \times 10^{-12}$ cm, respectively. During the refinement process, the scale factor, background function parameters (high-order polynominals), profile parameters *U*, *V*, *W*, and asymmetry coefficient, lattice parameters, atomic coordinates, and mean square displacement factors were refined. The Nd/Y site occupancies were fixed at the intended ratio of 0.4, 0.8, and 1.2 in $Ba(Nd_xY_{2-x})CuO_5$ for two reasons. Firstly the XRD Rietveld refinement results yielded the Nd content of the three samples basically at the intended *x* values of 0.399(3), 0.800(4), and 1.200(5), respectively. Secondly, the scattering lengths of Nd (0.769) and Y (0.775) are similar. The mean square displacement factors of the same atom types were constrained to be equal in the calculation.

2.4. Reference X-ray patterns for $Ba(Nd_xY_{2-x})CuO_5$ ($x = 0.8$ and 1.9)

The $Ba(Nd_xY_{2-x})CuO_5$ powders were mounted as acetone slurries in zero-background quartz holders. A Bruker D8 advance diffractometer equipped with a VANTEC-1 position-sensitive detector was used to measure the powder patterns (Cu$K\alpha$ radiation, 40 kV, 40 mA) from 5° to 150° 2θ in 0.007297° steps, counting for 0.5 s per step. Reference X-ray patterns were obtained with a Rietveld pattern decomposition technique. These patterns represent ideal specimen patterns. They are corrected for systematic errors both in *d*-spacing and intensity. The reported peak positions are calculated from the refined lattice parameters, as this represents the best measure of the true positions. For peaks resolved at the instrument resolution function, the individual peak positions are reported. For overlapping peaks, the intensity-weighted average peak position is reported with multiple indices. For marginally resolved peaks, individual peaks are reported to more accurately simulate the visual appearance of the pattern.

3. Results and discussion

Results of characterization of the $Ba(Nd_xY_{2-x})CuO_5$ solid solution are discussed in the following two sections: (1) solid solution range for $Ba(Nd_xY_{2-x})CuO_5$ using the Rietveld analysis technique; and (2) structural investigation of $Ba(Nd_xY_{2-x})CuO_5$ ($x = 0.4$, 0.8, 1.2) using NPD Rietveld refinement technique.

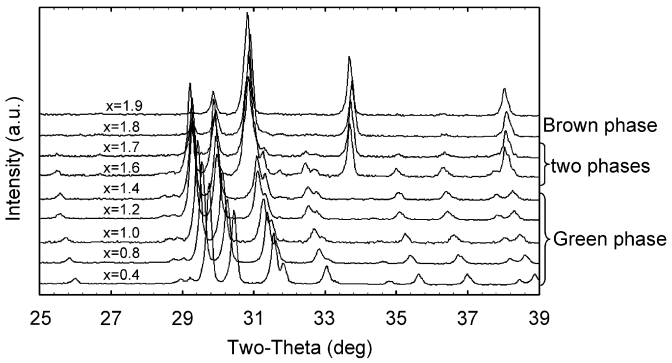

Fig. 1. XRD patterns for $Ba(Nd_xY_{2-x})CuO_5$ (samples prepared at 980 °C in air) showing two single phase regions ('brown phase' ($1.8 \leqslant x \leqslant 2.0$); 'green phase' ($1.4 < x < 1.8$). The two-phase region exhibits peaks from both the 'brown phase' and the 'green phase').

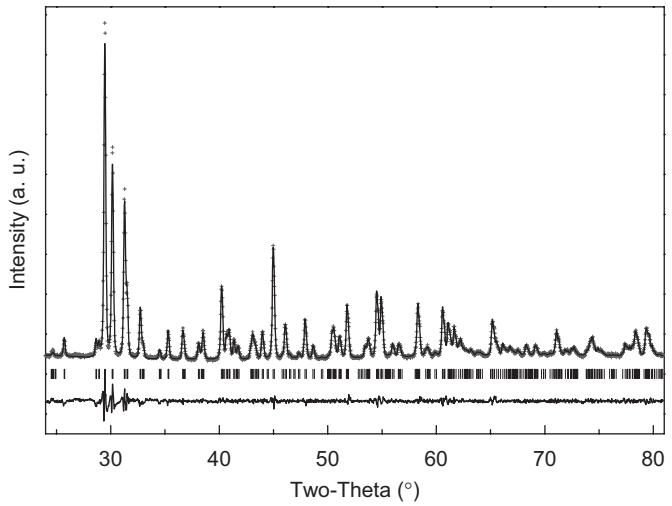

Fig. 2. Observed (crosses) and calculated (solid line) XRD pattern for $Ba(Nd_{0.8}Y_{1.2})CuO_5$ by Rietveld analysis technique. The difference pattern is plotted at same scale as the other patterns. The row of tick marks indicates the calculated peak positions.

Table 1
Refined lattice parameters of the orthorhombic 'green phase' (space group *Pnma*) in $Ba(Nd_xY_{2-x})CuO_5$ compounds; the average lattice parameters of BaY_2CuO_5 from 11 literature sources [17–27] are $a = 12.174(14)$ Å, $b = 5.657(3)$ Å, $c = 7.131(3)$ Å, $V = 491.28(71)$ Å^3

x	0.4		0.8		1.0	1.2		1.4	1.6	1.7
	XRD	NPD	XRD	NPD	XRD	XRD	NPD	XRD	XRD	XRD
a (Å)	12.264(4)	12.2629(3)	12.330 (5)	12.3408(4)	12.376(5)	12.409(4)	12.4094(6)	12.443(6)	12.439(4)	12.441(4)
b (Å)	5.687(2)	5.6870(1)	5.711(3)	5.7158(2)	5.731(2)	5.746(2)	5.7454(3)	5.763(3)	5.764(2)	5.769(2)
c (Å)	7.171(3)	7.1710(2)	7.206(3)	7.2123(2)	7.233(3)	7.255(3)	7.2563(4)	7.280(3)	7.279(2)	7.285(2)
V (Å^3)	500.1(3)	500.10(2)	507.5(4)	508.74(3)	513.0(3)	517.3(3)	517.35(4)	522.0(4)	521.9(3)	522.7(3)

Table 2
Refined lattice parameters of the tetragonal 'brown phase' (space group *P4/mbm*) in $Ba(Nd_xY_{2-x})CuO_5$ compounds; the lattice parameters of $BaNd_2CuO_5$ from PDF 42-0497 (ICDD) are $a = 6.6977$ Å, $c = 5.8209$ Å, $V = 261.12$ Å^3

x	1.6	1.7	1.8	1.9
a (Å)	6.686(2)	6.686(2)	6.691(3)	6.692(2)
c (Å)	5.821(2)	5.821(2)	5.820(3)	5.824(2)
V (Å^3)	260.2(2)	260.2(1)	260.6(2)	260.8(2)

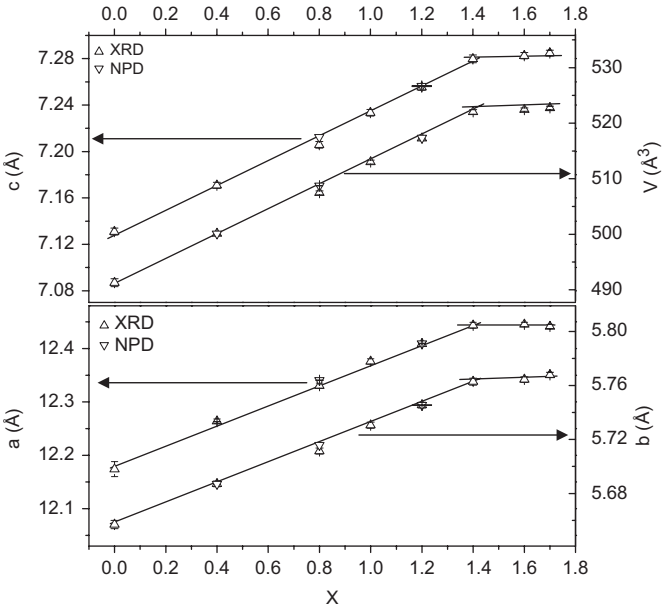

Fig. 3. Variation of lattice parameters and unit cell volume versus composition (x) in $Ba(Nd_xY_{2-x})CuO_5$. The data point at $x = 0$ refers to the average literature value for BaY_2CuO_5 [17–27].

3.1. Solid solution range for $Ba(Nd_xY_{2-x})CuO_5$

A complete solid solution of $Ba(Nd_xY_{2-x})CuO_5$ was not obtained under the current processing conditions. The XRD phase identification results showed that the regions for single phase solid solutions are $0 \leqslant x \leqslant 1.4$ for the 'green phase' structure, and $1.8 \leqslant x \leqslant 2$ for the 'brown phase' structure, respectively. These two phases have different chemistry and structure, despite similar stoichiometry. A two-phase region exists for $1.4 < x < 1.8$. X-ray diffraction patterns for the $Ba(Nd_xY_{2-x})CuO_5$ samples are presented in Fig. 1. All single phase samples for $0 \leqslant x \leqslant 1.4$ could be indexed by using the structure of the 'green phase', BaY_2CuO_5, which has the orthorhombic space group *Pnma* [21,22]. The sample $Ba(Nd_{1.9}Y_{0.1})CuO_5$ could be indexed by using the structure of the 'brown phase', $BaNd_2CuO_5$, which has the tetragonal space group *P4/mbm* [28].

Table 3
Refined structural parameters of $Ba(Nd_xY_{2-x})CuO_5$ ($y = \frac{1}{4}$ for Ba, Y/Nd, Cu, and O3) from NPD experiments (orthorhombic (*Pnma*))

x	0.4	0.8	1.2
Ba, x	0.9050(2)	0.9058(3)	0.9056(4)
z	0.9319(4)	0.9322(5)	0.9325(7)
U_{iso}	0.80(6)	0.87(9)	1.02(12)
Nd1/Y1, x	0.5740(2)	0.5734(2)	0.5735(3)
z	0.1045(2)	0.1057(3)	0.1072(4)
U_{iso}	0.62(3)	0.52(4)	0.53(5)
Nd2/Y2, x	0.7880(1)	0.7880(2)	0.7876(3)
z	0.3843(2)	0.3852(3)	0.3867(5)
U_{iso}	0.62(3)	0.52(4)	0.53(5)
Cu, x	0.6596(2)	0.6598(2)	0.6597(3)
z	0.7130(3)	0.7138(3)	0.7137(4)
U_{iso}	0.77(4)	0.69(5)	0.48(7)
O1, x	0.5684(2)	0.5685(2)	0.5687(3)
y	0.5080(3)	0.5074(4)	0.5096(7)
z	0.8329(2)	0.8313(2)	0.8304(4)
U_{iso}	0.72(4)	0.92(5)	0.75(7)
O2, x	0.7718(1)	0.7719(2)	0.7720(2)
y	0.5057(4)	0.5067(5)	0.5081(8)
z	0.6456(2)	0.6464(3)	0.6484(5)
U_{iso}	0.96(5)	0.85(7)	1.18(9)
O3, x	0.6002(2)	0.6000(3)	0.5983(3)
z	0.4216(4)	0.4241(4)	0.4257(6)
U_{iso}	1.04(8)	0.91(11)	0.82(15)
wR_p	0.0409	0.0469	0.0521
R_p	0.0345	0.0392	0.0429
χ^2	0.8998	1.051	0.9646
$R(F^2)$	0.0237	0.0363	0.0424

The lattice parameters of $Ba(Nd_xY_{2-x})CuO_5$ that are obtained from powder XRD data by Rietveld analysis (Fig. 2) are listed in Tables 1 and 2. As was expected, in the region $0 \leqslant x \leqslant 1.4$, because the ionic radius of Y^{3+} is smaller than that of Nd^{3+} [34], the 'green phase' lattice parameters, a, b, and c, of the unit cell and volume, V, increase monotonically as the amount of the Nd^{3+} (x) increases (Fig. 3). In the two-phase region of $1.4 < x < 1.8$, the lattice parameters of both the 'green phase' and 'brown phase' remain constant.

3.2. NPD structural investigation of orthorhombic $Ba(Nd_xY_{2-x})CuO_5$ ($x = 0.4, 0.8, 1.2$)

The refined positional and displacement (thermal) parameters using the NPD Rietveld technique for $Ba(Nd_xY_{2-x})CuO_5$ are given

in Table 3. As expected, the values of the final atomic coordinates for each atom type are rather similar in all four members of $Ba(Nd_xY_{2-x})CuO_5$, including BaY_2CuO_5 ($x=0$ [21]). It should be pointed out that in Table 3, the $\chi^2 \leqslant 1$ values are due to the relatively short data collection duration, i.e. 7.5 h for each data set (the normalized χ^2 function is simply the square of the ratio of R_{wp} to R_{exp}, where $R_{exp} \approx 1/(\langle y \rangle)^{1/2}$ and y is observed intensity [35]). Fig. 4 gives the observed and calculated NPD pattern for $Ba(Nd_{0.8}Y_{1.2})CuO_5$ at room temperature.

Fig. 5 presents a perspective view of the structure of $Ba(Nd_xY_{2-x})CuO_5$ ($0 \leqslant x \leqslant 1.4$) along the b-axis. $Ba(Nd_xY_{2-x})CuO_5$ ($0 \leqslant x \leqslant 1.4$) is confirmed to be isostructural to the 'green phase' BaR_2CuO_5 analogs [17–27]. The general structure of the 'green phase' $Ba(Nd_xY_{2-x})CuO_5$ consists of a three-dimensional network of interconnected $[(Nd,Y)O_7]$, $[BaO_{11}]$, and $[CuO_5]$ polyhedra. The copper ions are situated in distorted "square" pyramids $[CuO_5]$. The $[(Nd,Y)_2O_{11}]$ groups are formed from two monocapped trigonal $[(Nd,Y)O_7]$ prisms sharing a triangular face (Fig. 6). The Ba^{2+} ions are found to reside in distorted 11-fold coordinated cages (Fig. 6).

All ions were found to be located in layers formed by oxygen alternating with $[Ba(Nd,Y)_2CuO]$ that are perpendicular to the shortest b-axis. The $[(Nd,Y)O_7]$ prisms are stacked parallel to each other with shared trigonal faces or edges (Fig. 7), and can be viewed as sharing trigonal faces or edges to form wavelike chains parallel to the long x-axis (Figs. 6 and 7). The chains are then linked by the distorted "square" pyramids $[CuO_5]$ with shared trigonal faces or edges (Fig. 7) to form two-dimensional network layer at $y=1/4$. The $[(Nd,Y)O_7]$ and $[CuO_5]$ polyhedra of the second layer at $y=3/4$ share edges with the $[(Nd,Y)O_7]$ and $[CuO_5]$ polyhedra of the first layer to form a three-dimensional network whose cages are occupied by Ba ions (Fig. 5).

Selected interatomic distances for $Ba(Nd_xY_{2-x})CuO_5$ are listed in Table 4. Because the ionic radius of the Y^{3+} ion (1.019 Å) is substantially smaller than that of the Nd^{3+} ion (1.109 Å) [33], the change in the (Nd,Y)–O bond length with "x" is apparent, which in turns affect the size of the (Nd,Y)- and the Ba-cages. It is this notable lengthening of the (Nd,Y)–O bonds that is primarily

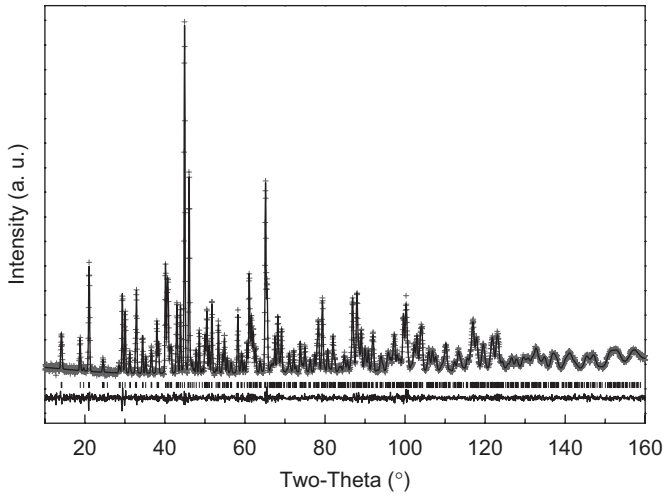

Fig. 4. Observed (crosses) and calculated (solid line) NPD intensities pattern for $Ba(Nd_{0.8}Y_{1.2})CuO_5$ at 295 K The difference pattern is plotted at same scale as the other patterns. The row of tick marks indicates the calculated peak positions.

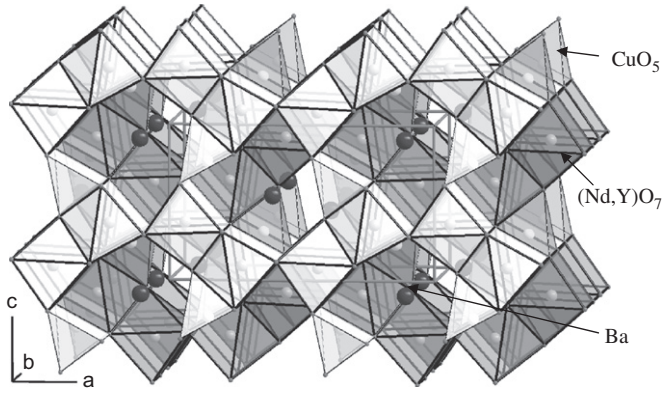

Fig. 5. Perspective view of the orthorhombic 'green phase' $Ba(Nd_xY_{2-x})CuO_5$ structure along the b-axis, showing the isolated square pyramids of $[CuO_5]$ and the trigonal RO_7 prisms around the rare-earth atoms.

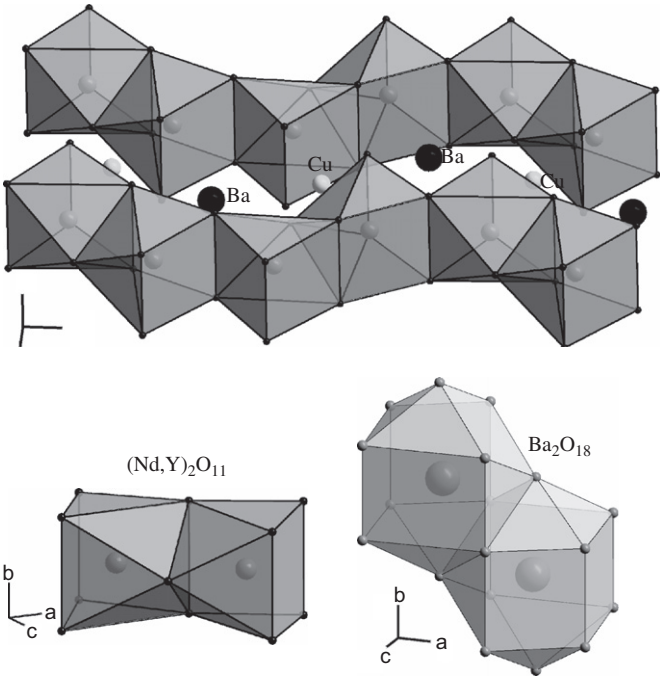

Fig. 6. Coordination environments of $(Nd,Y)_2O_{11}$ formed by two $(Nd,Y)O_7$ groups and Ba_2O_{18} formed by two BaO_{11} units found in the orthorhombic 'green phase' $Ba(Nd_xY_{2-x})CuO_5$ structure.

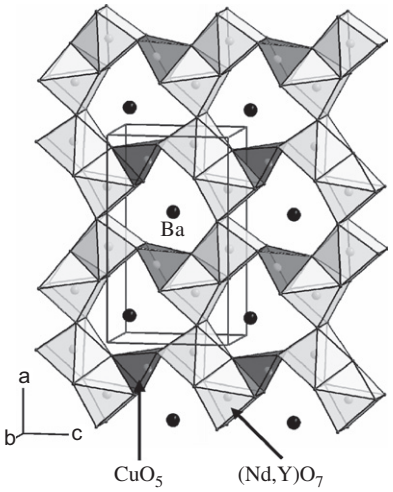

Fig. 7. Projection of the structure of the orthorhombic 'green phase' $Ba(Nd_xY_{2-x})CuO_5$ along b at $y=1/4$.

Table 4
Selected bond distances (Å) in orthorhombic $Ba(Nd_xY_{2-x})CuO_5$ compounds

x	0.4	0.8	1.2
Ba			
–O1 × 2	3.085(3)	3.093(4)	3.105(5)
–O1 × 2	3.245(3)	3.248(4)	3.265(5)
–O2 × 2	2.969(3)	2.986(4)	2.988(6)
–O2 × 2	3.026(3)	3.057(4)	3.084(5)
–O3 × 1	2.615(4)	2.612(5)	2.603(6)
–O3 × 2	2.845(2)	2.859(0)	2.874(0)
Y1/Nd1			
–O1 × 2	2.386(2)	2.417(3)	2.438(4)
–O1 × 2	2.324(2)	2.333(3)	2.355(4)
–O2 × 2	2.404(3)	2.426(3)	2.442(5)
–O3 × 1	2.297(3)	2.320(4)	2.331(5)
Y2/Nd2			
–O1 × 2	2.322(2)	2.335(3)	2.360(4)
–O2 × 2	2.342(3)	2.349(3)	2.360(5)
–O2 × 2	2.362(3)	2.381(3)	2.396(5)
–O3 × 1	2.318(3)	2.337(4)	2.366(5)
Cu			
–O1 × 2	1.972(2)	1.977(3)	1.975(4)
–O2 × 2	2.014(2)	2.021(3)	2.025(5)
–O3 × 1	2.213(3)	2.216(4)	2.225(5)

Table 5
Bond valence sum (V_b) in $Ba(Nd_xY_{2-x})CuO_5$ [36,37]

x	0.4	0.8	1.2
Ba	1.81	1.76	1.72
Y1/Nd1	2.94	2.92	2.91
Y2/Nd2	3.11	3.14	3.13
Cu	1.95	1.92	1.91

responsible for the apparent increase of the lattice parameters with increasing Nd^{3+} content (x).

The bond valence sum values, V_b, for Ba, Y, and Cu were calculated using the Brown–Altermatt empirical expression [36,37], and the results are listed in Table 5. The V_b of an atom i is defined as the sum of the bond valences v_{ij} of all the bonds from atoms i to atoms j. The most commonly adopted empirical expression for the bond valence v_{ij} as a function of the interatomic distance d_{ij} is

$$v_{ij} = \exp[(R_0 - d_{ij})/B].$$

The parameter, B, is commonly taken to be a "universal" constant equal to 0.37 Å. The values of the reference distance R_0 for Ba–O, Cu–O, Nd–O and Y–O are 2.285, 1.679, 2.118 and 2.019 Å, respectively [36,37]. In Table 5, note that while the V_b values for Cu, and Nd/Y in all three $Ba(Nd_xY_{2-x})CuO_5$ solid solution members are close to the ideal values of 2 and 3, respectively; small compressive stress increases in the $R1$ and Cu sites as Nd site occupancy increases from 0.4 to 1.2. On the other hand, for the $R2$ site, small tensile stress increases as x increases. The V_b values for the Ba site are all significantly less than the ideal value of 2 (underbonding, tensile stress, or atom in an oversized cage), they decrease from 1.8145 ($x = 0.4$) to a small value of 1.7199 ($x = 1.2$).

Tables 6 and 7 give the X-ray powder reference patterns for $Ba(Nd_{1.9}Y_{0.1})CuO_5$, and for $Ba(Nd_{0.8}Y_{1.2})CuO_5$. These reference patterns have been submitted to the International Centre for Diffraction Data (ICDD) to be included in the PDF. In these tables, the symbols M and $+$ refer to peaks containing contributions from two and more than two reflections, respectively. The symbol * indicates the particular peak has the strongest intensity of the entire pattern and is designated a value of '999'. The intensity values reported are integrated intensities rather than peak heights.

Table 6
X-ray reference pattern for $Ba(Nd_{1.9}Y_{0.1})CuO_5$, $P4/mbm$ (no. 127), $a = 6.69120\ (4)$ Å, $c = 5.81839\ (4)$ Å, $V = 260.50$ Å^3

d (Å)	I	h	k	l	d (Å)	I	h	k	l	d (Å)	I	h	k	l
5.8184	83	0	0	1	4.7314	11	1	1	0	3.6709	161	1	1	1
2.9924	259	2	1	0	2.9092	395	0	0	2	2.9003	999*	2	0	1
2.6611	614	2	1	1	2.4782	12	1	1	2	2.3657	261	2	2	0
2.1953	14	2	0	2	2.1915	29	2	2	1	2.1159	267	3	1	0
2.0859	455	2	1	2	1.9885	26	3	1	1	1.8558	9	3	2	0
1.8354	224	2	2	2	1.7946	36	1	1	3	1.7112	145	3	1	2
1.6779	231	2	0	3	1.6275	133	2	1	3	1.6229	86	4	1	0
1.6077	130	4	0	1	1.5771	47	3	3	0	1.5632	189	4	1	1
1.5222	180	3	3	1	1.4999	12	2	2	3	1.4962	108	4	2	0
1.4546	89	0	0	4	1.4495	69	4	0	2M	1.4495	69	4	2	1M
1.4297	15	3	1	3	1.4173	141	4	1	2	1.3865	31	3	3	2
1.3305	118	4	2	2	1.3082	51	2	1	4	1.2801	44	5	1	1
1.2667	62	4	0	3	1.2446	79	4	1	3	1.2425	12	5	2	0
1.2391	62	2	2	4	1.2236	86	3	3	3	1.2151	45	5	2	1
1.1987	75	3	1	4	1.1846	18	4	2	3	1.1829	25	4	4	0
1.1591	15	4	4	1	1.1475	44	5	3	0	1.1427	52	5	2	2
1.1300	8	1	1	5	1.1258	19	5	3	1	1.1152	69	6	0	0
1.0991	59	2	0	5	1.0956	24	4	4	2M	1.0956	24	6	0	1M
1.0869	22	5	1	3	1.0846	46	2	1	5	1.0832	49	4	1	4
1.0693	24	3	3	4	1.0675	85	5	3	2	1.0462	26	5	2	3
1.0450	16	5	4	0	1.0430	63	4	2	4	1.0411	204	6	0	2M
1.0411	204	6	2	1M	1.0285	44	5	4	1	1.0197	5	3	1	5
1.0099	13	4	4	3	0.9943	5	6	2	2	0.9876	18	5	3	3
0.9835	44	5	4	2	0.9697	23	0	0	6	0.9668	5	6	0	3
0.9553	31	4	0	5	0.9457	52	4	1	5	0.9448	17	5	2	4
0.9364	52	3	3	5	0.9340	27	7	1	1M	0.9340	27	5	5	1M
0.9288	101	6	2	3	0.9225	47	2	1	6	0.9200	35	5	4	3
0.9191	25	7	2	0	0.9186	11	4	2	5	0.9177	30	4	4	4
0.9163	65	6	4	1	0.9079	54	7	2	1	0.9009	71	5	3	4
0.8999	5	7	1	2	0.8973	37	2	2	6	0.8850	111	6	0	4
0.8840	10	6	4	2	0.8816	38	3	1	6	0.8786	16	7	3	0
0.8774	7	6	1	4	0.8764	50	7	2	2	0.8707	27	5	1	5

Table 6 (*continued*)

d (Å)	*I*	*h*	*k*	*l*	*d* (Å)	*I*	*h*	*k*	*l*	*d* (Å)	*I*	*h*	*k*	l
0.8567	5	6	5	0	0.8505	33	7	1	3M	0.8504	33	5	5	3M
0.8494	37	5	2	5	0.8487	39	5	4	4	0.8411	15	7	3	2
0.8390	7	4	0	6	0.8370	82	6	4	3	0.8324	71	4	1	6
0.8306	64	7	2	3	0.8299	54	7	4	0M	0.8299	54	8	1	0M
0.8295	11	4	4	5	0.8279	91	8	0	1	0.8261	19	3	3	6
0.8216	136	7	4	1M	0.8216	136	8	1	1M	0.8187	13	1	1	7
0.8171	21	5	3	5	0.8138	81	4	2	6	0.8114	70	8	2	0
0.8067	87	2	0	7	0.8052	9	6	0	5	0.8009	62	2	1	7
0.7981	175	8	1	2M	0.7981	175	7	4	2M					

The symbol '*d*' refers to *d*-spacing values, '*I*' refers to *I* integrated intensity value (scaled according to the maximum value of 999; the symbol* indicates the strongest peak), the *h k l* values are the Miller indexes, M and + refer to peaks containing contributions from two and more than two reflections, respectively.

Table 7
X-ray reference pattern for $Ba(Nd_{0.8}Y_{1.2})CuO_5$, *Pnma* (no. 62), $a = 12.220\ (5)$ Å, $b = 5.711(3)$ Å, $c = 7.206(3)$ Å, $V = 507.5(4)$ Å^3

d (Å)	*I*	*h*	*k*	*l*	*d* (Å)	*I*	*h*	*k*	*l*	*d* (Å)	*I*	*h*	*k*	*l*
6.1701	8	2	0	0	4.6883	7	2	0	1	4.4795	13	0	1	1
3.6058	14	0	0	2	3.4611	39	1	0	2	3.1132	56	2	0	2
3.0850	48	4	0	0	3.0298	999*	3	1	1	2.9606	652	1	1	2
2.8580	433	0	2	0	2.8364	181	4	0	1	2.7340	140	2	1	2
2.7144	35	4	1	0M	2.7144	35	3	0	2M	2.5974	17	1	2	1
2.5408	75	4	1	1	2.4498	74	3	1	2	2.4403	17	2	2	1
2.3595	42	1	0	3	2.3442	7	4	0	2	2.3351	75	5	0	1
2.2399	220	2	0	3M	2.2399	220	0	2	2M	2.2159	59	0	1	3
2.2038	73	1	2	2	2.1810	51	1	1	3	2.1688	5	4	1	2
2.1617	32	5	1	1	2.1053	23	2	2	2	2.0966	59	4	2	0
2.0855	30	2	1	3	2.0567	80	6	0	0	2.0132	312	4	2	1
1.9778	5	6	0	1	1.9671	86	3	2	2	1.9508	11	3	1	3
1.9185	13	5	1	2	1.8962	113	4	0	3	1.8691	34	6	1	1
1.8195	5	1	2	3	1.8083	64	5	2	1	1.8029	46	0	0	4
1.7998	17	4	1	3	1.7865	38	6	0	2	1.7840	31	1	0	4
1.7630	158	2	2	3	1.7125	34	7	0	1	1.7052	5	6	1	2
1.7030	52	1	1	4	1.6812	178	3	3	1	1.6692	165	6	2	0M
1.6692	165	1	3	2M	1.6488	6	5	1	3	1.6404	39	7	1	1
1.6254	37	6	2	1M	1.6254	37	2	3	2M	1.6211	6	4	3	0
1.5837	6	7	0	2	1.5816	19	4	3	1	1.5801	132	4	2	3
1.5628	15	6	0	3	1.5589	19	3	3	2	1.5425	12	8	0	0
1.5260	151	7	1	2M	1.5260	151	0	2	4M	1.5149	69	6	2	2
1.5133	26	1	2	4	1.5084	11	8	0	1	1.5019	84	4	1	4
1.4932	18	0	3	3	1.4893	43	8	1	0	1.4824	15	1	3	3
1.4762	10	5	3	1	1.4690	16	7	2	1	1.4585	11	8	1	1
1.4513	9	2	3	3	1.4326	5	1	0	5	1.4291	108	3	2	4M
1.4291	108	0	4	0M	1.4216	31	7	0	3	1.4108	33	5	1	4
1.4045	9	2	0	5	1.3985	27	0	1	5	1.3914	5	5	3	2
1.3853	16	7	2	2	1.3715	34	6	3	1M	1.3715	34	6	2	3
1.3611	5	3	0	5	1.3574	10	8	2	0	1.3558	24	6	0	4
1.3440	8	4	3	3	1.3340	9	8	2	1	1.3240	81	3	1	5
1.3208	7	1	4	2	1.3111	21	9	1	1	1.3022	20	1	3	4
1.2966	5	4	4	0	1.2807	14	1	2	5	1.2762	36	4	4	1
1.2733	34	7	3	1+	1.2660	19	8	1	3	1.2605	9	2	2	5
1.2453	5	5	0	5	1.2340	5	10	0	0	1.2309	34	7	1	4
1.2288	5	3	2	5	1.2249	20	6	2	4	1.2223	9	1	4	3
1.2189	17	5	4	1	1.2179	60	7	3	2	1.2052	93	2	4	3+
1.2019	10	0	0	6	1.1989	20	8	3	0	1.1826	6	8	3	1
1.1735	23	6	4	0	1.1721	5	8	0	4	1.1675	9	10	0	2
1.1567	24	5	3	4M	1.1567	24	6	1	5M	1.1537	19	3	0	6
1.1500	14	0	3	5	1.1416	6	5	2	5	1.1412	41	4	4	3
1.1329	11	10	2	0	1.1196	32	0	4	4M	1.1196	32	10	2	1M
1.1158	31	6	4	2+	1.1077	83	3	3	5+	1.0999	12	9	3	1
1.0978	18	10	0	3	1.0972	14	7	4	1	1.0887	58	3	5	1M
1.0887	58	11	1	1M	1.0855	30	1	5	2	1.0844	8	8	2	4
1.0808	11	10	2	2	1.0730	18	2	5	2M	1.0730	18	8	3	3M
1.0720	7	9	1	4	1.0712	19	11	0	2	1.0698	36	3	2	6
1.0546	8	6	4	3	1.0535	12	8	0	5M	1.0535	12	3	5	2M
1.0512	19	7	3	4	1.0483	6	8	4	0	1.0398	14	7	2	5
1.0377	6	6	0	6	1.0358	9	10	3	0	1.0335	7	11	2	1
1.0324	5	0	5	3	1.0267	6	1	0	7	1.0248	34	10	2	3
1.0139	20	0	1	7	1.0121	8	12	1	0	1.0078	19	7	4	3
1.0037	6	6	3	5	1.0031	45	11	2	2	1.0025	13	10	1	4
1.0017	6	2	4	5	0.9885	19	8	2	5	0.9844	5	3	1	7
0.9835	16	6	4	4	0.9784	19	7	1	6	0.9772	11	4	0	7

Table 7 (*continued*)

d (Å)	*I*	*h*	*k*	*l*	*d* (Å)	*I*	*h*	*k*	*l*	*d* (Å)	*I*	*h*	*k*	*l*
0.9754	24	6	2	6	0.9662	8	1	2	7	0.9625	10	1	5	4
0.9593	7	10	2	4	0.9581	8	11	3	1	0.9527	20	0	6	0
0.9508	8	7	5	1	0.9470	5	9	3	4	0.9434	5	3	2	7
0.9395	8	11	1	4	0.9388	5	5	4	5	0.9381	7	7	2	6
0.9353	5	8	1	6	0.9340	6	10	4	0	0.9286	14	13	1	1
0.9269	34	7	5	2	0.9253	7	10	1	5	0.9246	14	4	2	7
0.9214	23	4	5	4	0.9198	12	0	4	6	0.9185	15	1	6	2M
0.9185	15	8	5	0M	0.9094	13	6	1	7	0.9063	39	0	3	7+
0.9050	8	12	3	0	0.9041	10	10	4	2	0.9031	29	4	6	1
0.8990	22	5	5	4M	0.8990	22	3	6	2M	0.8978	41	10	3	4M
0.8978	41	3	4	6M	0.8960	8	0	5	5	0.8881	10	1	1	8

The symbol '*d*' refers to *d*-spacing values, '*I*' refers to *I* integrated intensity value (scaled according to the maximum value of 999; the symbol* indicates the strongest peak), the *h k l* values are the Miller indexes, M and + refer to peaks containing contributions from two and more than two reflections, respectively.

4. Summary

Structure and morphology of grains of BaR_2CuO_5 are some of the factors that needed to be considered for it to be an effective flux-pinning agent for coated conductor applications. The orthorhombic 'green phase' BaR_2CuO_5 and tetragonal 'brown phase' BaR_2CuO_5 compounds have totally different chemistry and different structure. So far only the orthorhombic 'green phase' BaR_2CuO_5 have been found to be effective in flux-pinning applications. As the tetragonal $BaNd_2CuO_5$ and orthorhombic BaY_2CuO_5 phases and their intermediate solid solution members, $Ba(Nd_xY_{2-x})CuO_5$, adopt two different structure types due to different average ionic size of the lanthanide sites, we found that it is necessary to determine the structure and crystal chemistry of the solid solution members using XRD and NPD technologies. In the solid solution members that have a majority of Nd as compared to Y, the mixed-lanthanide sites have a relatively large ionic radius and they adopt an 8-coordination environment ($(Nd,Y)O_8$), resulting in the 'brown phase' $Ba(Nd,Y)_2CuO_5$ structure [28]. In the case of the 'green phase' type structure (the lanthanide site has a majority of Y) where the average ionic size of (Nd,Y) is relatively smaller, (Nd,Y) adopts a monocapped trigonal prism environment, $(Nd,Y)O_7$ [20–22]. We found the $Ba(Nd_xY_{2-x})CuO_5$ series consists of a Nd-rich tetragonal solid solution, a Y-rich orthorhombic solid solution and a two-phase region in between. We have also provided the X-ray powder reference patterns for two selected members of the orthorhombic 'green phase' $Ba(Nd_xY_{2-x})CuO_5$ members.

It is estimated that research interest on mixed-lanthanide-coated conductors will continue for some time, therefore further structural characterizations of different mixed-lanthanide members of $Ba(R,R')_2CuO_5$ to distinguish the orthorhombic from tetragonal are needed for flux-pinning applications.

Acknowledgments

The authors are grateful for the partial financial support from the Department of Energy (DOE) and the International Centre for Diffraction Data.

References

[1] A.P. Malozemoff, D.T. Verebelyi, S. Fleshler, D. Aized, D. Yu, Physica C 385 (2003) 424–430.
[2] H.S. He, H.S. Kim, J.S. Yang, Y.H. Jung, R.K. Ko, K.J. Song, D.W. Ha, S.S. Oh, H.K. Kim, K.K. Yoo, S.I. Yoo, C. Park, D.J. Youm, S.H. Moon, J.H. Joo, Physica C 463–465 (2007) 493–496.
[3] M.W. Rupich, W. Zhang, X. Li, T. Kodenkandath, D.T. Verebelyi, U. Schoop, C. Thieme, M. Teplitsky, J. Lynch, N. Nguyen, E. Siegal, J. Scudiere, V. Maroni, K. Venkataraman, D. Miller, T.G. Holesinger, Physica C 412–414 (2004) 877–884.
[4] A. Goyal, D.P. Norton, J.D. Budai, M. Paranthaman, E.D. Specht, D.M. Kroeger, D.K. Christen, Q. He, B. Saffian, F.A. List, D.F. Lee, P.M. Martin, C.E. Klabunde, E. Hartfield, V.K. Sikka, Appl. Phys. Lett. 69 (1996) 1795–1797.
[5] A. Goyal, U. Schoop, P. Paranthaman, MRS Bull. 29 (2004) 552–563.
[6] P.N. Arendt, S.R. Foltyn, L. Civale, R.F. DePaula, P.C. Dowden, J.R. Groves, T.G. Holesinger, Q.X. Jia, S. Kreiskott, L. Stan, I. Usov, H. Wang, J.Y. Coulter, Physica C 412–414 (2004) 795–800.
[7] S.R. Foltyn, E.J. Peterson, J.Y. Coulter, P.N. Arendt, Q.X. Jia, P.C. Dowden, M.P. Maley, X.D. Wu, D.E. Peterson, J. Mater. Res. 12 (1997) 2941–2946.
[8] Y. Yamada, A. Ibi, H. Fukushima, R. Kuriki, S. Miyata, K. Takahashi, H. Kobayashi, S. Ishida, M. Konishe, T. Kato, T. Hirayama, Y. Shiohara, Physica C 445–448 (2006) 504–508.
[9] R. Feenstra, T.B. Lindemer, J.D. Budai, M.D. Galloway, J. Appl. Phys. 69 (1991) 6569.
[10] R. Feenstra, US Patent 5,972,847, 1999.
[11] V. Selvamanickam, H.G. Lee, Y. Li, X. Xiong, Y. Qiao, J. reeves, Y. Xie, A. Knoll, K. Lenseth, Physica C 392–396 (2003) 859–862.
[12] V. Selvamanickam, Y. Chen, X. Xiong, Y.Y. Xie, J.L. Reeves, X. Zhang, Y. Qiao, K.P. Lenseth, R.M. Schmidt, A. Rar, D.W. Hazelton, K. Tekletsadik, IEEE Trans. Appl. Superconduct. 17 (2) (2007) 3231–3234.
[13] P.M. Mankiewich, J.H. Scofield, W.J. Skocpol, R.E. Howard, A.H. Dayem, E. Good, Appl. Phys. Lett. 51 (21) (1987) 1753.
[14] S.-W. Chan, B.G. Bagley, L.H. Greene, M. Giroud, W.L. Feldmann, K.R. Jenkin II, B.J. Wilkins, Appl. Phys. Lett. 53 (15) (1988) 1443.
[15] P.C. McIntyre, M.J. Cima, J. Mater. Res. 9 (9) (1994) 2219.
[16] P.C. McIntyre, M.J. Cima, A. Roshko, J. Appl. Phys. 77 (10) (1995) 5263.
[17] C. Michel, B. Raveau, J. Solid State Chem. 43 (1982) 73–80.
[18] N.L. Ross, R.J. Angel, L.W. Finger, R.M. Hazen, C.T. Prewitt, ACS Symp. Ser. 351 (1987) 164–172.
[19] H. Fjellvag, P. Karen, P.A. Kjekshus, Acta Chem. Scand. 41 (1987) 283–293.
[20] R.M. Hazen, L.W. Finger, R.A. Angel, C.T. Prewitt, N.L. Ross, H.K. Mao, C.G. Hadidiacos, Phys. Rev. B 35 (1987) 7238–7241.
[21] S.F. Watkins, R.R. Fronczek, K.S. Wheelock, R.G. Goodrich, W.O. Hamilton, W.W. Johnson, Acta Crystallogr. C 44 (1988) 3–6.
[22] W. Wong-Ng, M.A. Kuchinski, H.F. McMurdie, B. Paretzkin, Powder Diffr. 4 (1989) 2–8.
[23] S. Sato, I. Nakada, Acta Crystallogr. C 45 (1989) 523–525.
[24] B.A. Hunter, S.L. Town, R.L. Davis, G.J. Russell, K.N.R. Taylor, Physica C 161 (1989) 594–597.
[25] A. Salinas-Sanchez, J.L. Garcia-Munoz, J. Rodriguez-Carvajal, R. Saez-Puche, J.L. Martinez, J. Solid State Chem. 100 (1992) 201–211.
[26] R.H. Buttner, E.N. Maslen, Acta Crystallogr. 49 (1993) 62–66.
[27] R. Hsu, E.N. Maslen, N. Ishizawa, Acta Crystallogr. 52 (1996) 569–572.
[28] J. Stalick, W. Wong-Ng, Mater. Lett. 9 (10) (1990) 401.
[29] D.N. Mattews, J.W. Cochrane, G.J. Russell, Physica C 249 (1995) 255–261.
[30] T. Haugan, P.N. Barnes, R. Wheeler, F. Meisenkothen, M. Sumption, Nature 430 (2004) 867–870.
[31] ICDD (International Centre for Diffraction Data), 12 Campus Blvd., Newtown Square, PA 19081, USA.
[32] J. Rodriguez-Carvajal, FULLPROF, 2k code, Version 3.3, 2005, 〈http://www-llb.cea.fr/fullweb/powder.htm〉.
[33] A.C. Larson, R.B. von Dreele, GSAS—general structure analysis system, US Government contract (W-7405-ENG-36) by the Los Alamos National laboratory, which is operated by the University of California for the US Department of Energy, 1992.
[34] R.D. Shannon, Acta Crystallogr. 32 (1976) 751–767.
[35] W.I.F. David, J. Res. Natl. Inst. Stand. Technol. 109 (2004) 107–123.
[36] N.E. Brese, M. O'Keeffe, Acta Crystallogr. 47 (1991) 192–197.
[37] I.D. Brown, D. Altermatt, Acta Crystallogr. 41 (1985) 244–247.